Aleksandar Dolashki, Lyudmila Velkova*, Wolfgang Voelter and Pavlina Dolashka

Structural and conformational stability of hemocyanin from the garden snail *Cornu aspersum*

https://doi.org/10.1515/znc-2018-0084
Received June 10, 2018; revised January 23, 2019; accepted February 2, 2019

Abstract: Various aspects of biomedical applications of molluscan hemocyanins, associated with their immunogenic properties and antitumor activity, promoted us to perform structural studies on these glycoproteins. The stability and reassociation behavior of native *Cornu aspersum* hemocyanin (CaH) are studied in the presence of different concentrations of Ca^{2+} and Mg^{2+} ions and pH values using electron microscopy. Higher concentrations of those ions led to a more rapid reassociation of CaH, resulting in stable multidecamers with different lengths. The conformational changes of native CaH are investigated within a wide pH-temperature range by UV circular dichroism. The relatively small changes of initial $[\theta]_{\lambda}$ indicated that many secondary structural elements are preserved, even at high temperatures above 80 °C, especially at neutral pH. The mechanism of thermal unfolding of CaH has a complicated character, and the process is irreversible. The conformational stability of the native didecameric aggregates of CaH toward various denaturants indicates that hydrophilic and polar forces stabilize the quaternary structure. For the first time, the unfolding of native CaH in water solutions in the presence of four different denaturants is investigated. The free energy of stabilization in water, $\Delta G_D^{H_2O}$, was calculated in the range of 15.48–16.95 kJ mol^{-1}. The presented results will facilitate the further investigation of the properties and potential applications of CaH.

Keywords: circular dichroism spectroscopy; conformational stability; *Cornu aspersum* hemocyanin; free energy of stabilization in water.

***Corresponding author: Lyudmila Velkova,** Institute of Organic Chemistry with Centre of Phytochemistry, Bulgarian Academy of Sciences, Acad. G. Bonchev str., bl.9, Sofia 1113, Bulgaria, E-mail: lyudmila_velkova@abv.bg
Aleksandar Dolashki and Pavlina Dolashka: Institute of Organic Chemistry with Centre of Phytochemistry, Bulgarian Academy of Sciences, Acad. G. Bonchev str., bl.9, Sofia 1113, Bulgaria
Wolfgang Voelter: Interfacultary Institute of Biochemistry, University of Tübingen, Hoppe-Seyler-Straße 4, D-72076 Tübingen, Germany

1 Introduction

Hemocyanins (Hcs) are oligomeric blue copper-containing respiratory proteins with extremely high molecular weight and complex quaternary structure found in the hemolymph of many arthropods and molluscs [1–3]. Hcs present in invertebrate hemolymph are multifunctional proteins performing various immunological and biological functions. Most molluscan Hcs are glycoproteins and possess immunotherapeutic potentials including antineoplastic, antiviral and antibacterial effects [4–10]. Some molluscan Hcs have a significant potential for new drug development [10, 11]. Recently, it has been reported that *Rapana venosa*, *Helix lucorum* and *Helix aspersa* Hcs display antitumor and antimicrobial activities [4, 7–9]. *Haliotis tuberculata* hemocyanin (HtH) contains encrypted antimicrobial peptides and may act as a source of antiinfective peptides [12].

The majority of molluscan Hcs are observed as hollow cylindrical decamers, didecamers or tridecamers, usually with molecular weights between 4 and 9 MDa [1–3, 5]. The basic molluscan Hc quaternary structure is decameric, a cylinder of 35–38 nm, containing 10 subunits with identical sequence [1, 2]. In recent years, there is a progress on structural investigation of molluscan Hcs [5, 13, 14]. An unusual gastropod Hc tridecamer was found in fresh/brackish water cerithioid snails, termed "mega-Hc" [13]. Mega-Hcs with a molecular mass of 13.5 MDa are among the largest known oxygen transporters found in the hemolymph of some snails [5, 13, 14]. The mega-Hcs from cerithioid snails are an exception, as their internal structure shows a more complex arrangement [5]. Molluscan Hc subunits are among the largest polypeptides found in nature [2], typically composed of about 400 amino acid residues with different sequences and genomic patterns and molecular masses of 330–450 kDa, depending on the species [1, 3]. The number of Hc isoforms present in molluscan species varies between 1 and 3 [1–3]. While marine gastropods have one or two structurally and functionally distinct Hc isoforms, three Hc isoforms (β-HlH, αD-HlH and αN-HlH) were reported for *H. lucorum* as well as *Helix pomatia* and *H. aspersa* [4, 15–17]. The subunit is folded into seven or eight different globular functional units (FUs) of ~50 kDa [2, 3]. Each FU contains one binuclear

copper active site, capable of reversibly binding one dioxygen molecule [1–3]. An additional feature of Hc structures are their carbohydrate contents, which play fundamental roles in their organization and their immunological efficacy [1, 3]. Gastropod Hcs are glycoproteins with a higher carbohydrate content of about 9% (w/w) than arthropod Hcs and may contain unusual monosaccharides, such as a methylated hexoses (for example, *O*-methylmannose and *O*-methylgalactose), β(1,2)-linked xylose, α(1,3)-linked fucose, α(1,6)-linked fucose or hexuronic acid [3, 7, 8]. To ensure the quality and effectiveness of the glycoprotein for therapeutic uses, its molecular structure and thermal stability are key characteristics that need elucidation.

In the literature, there is a limited number of publications on the biophysical properties and stability of molluscan Hcs. The association-dissociation properties of some molluscan and arthropod Hcs together with the conformational stability of Hcs under various physical conditions (i.e. temperature, pH and etc.) and/or chemical agents have been studied [18–27]. The equilibrium state of the native folded protein must therefore be regarded as representing a delicate balance between a large number of weak interactions, each of which is sensitive to temperature and the state of the surrounding solvent (i.e. pH, ionic strength, presence of hydrogen bond-breaking solutes such as urea, and presence of amphiphilic compounds which affect the balance of hydrophobic and hydrophilic interactions). Denaturation can be brought about in many ways, including thermal denaturation (by raising the temperature), denaturation by pH change and chemical denaturation. However, such studies may be complicated by the fact that it may be difficult to distinguish between the effects on the quaternary structure of the oligomeric proteins (i.e. initial dissociation) and those on the tertiary and secondary structures (i.e. subunit unfolding).

The main aim of this study was to determine the association-dissociation behavior and conformational stability of native Hcs isolated from the garden snail *Cornu aspersum* toward pH, temperature and different denaturants: guanidine hydrochloride (Gdn.HCl), urea, lithium chloride (LiCl) and urea + LiCl, monitored by UV circular dichroism (CD).

2 Materials and methods

2.1 Isolation of *C. aspersum* Hc

The hemolymph was collected from the foot of the *C. aspersum* snail, grown in Bulgarian eco-farms from northwestern Bulgaria. The hemolymph from a typical mollusc appears blue in color due to the presence of Hc as its major component (~90%) [5]. The native *C. aspersum* hemocyanin (CaH) (molecular mass of about 9000 kDa), containing two α-subunits (αD-CaH and αN-CaH) and one β-subunit (β-CaH), was isolated and purified from the hemolymph of the garden snail *C. aspersum* as described previously [4].

2.2 Electron microscopy

The stability and reassociation behavior of CaH were studied in the presence of different concentrations of Ca^{2+} and Mg^{2+} ions and pH by transmission electron microscopy (TEM). Electron micrographs were taken with a Philips®CM10 (Philips Electron Optics, Eindhoven, The Netherlands) transmission electron microscope with a 30-mm objective aperture. CaH samples were adsorbed for 60 s to a glow-discharged pistoform/carbon-coated support film, washed three times with droplets of distilled water to remove buffer salts and finally negatively stained with 1% uranyl acetate. Electron micrographs were routinely recorded at an instrumental magnification of ×45,000.

2.3 CD measurements

CD spectra were recorded with a J-720 spectropolarimeter (Jasco, Tokyo, Japan). Cylindrical temperature-controlled quartz cells with a path length of 5 mm were used in all the experiments. CD spectra were recorded in the UV range between 200 and 250 nm at 0.2-nm intervals with a bandwidth of 1 nm, a scan speed of 50 nm/min and a time constant of 8.0 s. The specific absorption coefficient $\varepsilon_{278nm} = 1.413$ mL mg^{-1} cm^{-1} [15] was used for determining the protein concentration. Protein solutions were prepared in 20 mM "cocktail buffer" [by equal stocks of 20 mM sodium phosphate buffer (pH 7.4–5.5), 20 mM sodium acetate buffer (pH 5.4–3.6) and 20 mM Tris-HCl buffer (6.4–11.0)] in the presence of 5 mM $CaCl_2$. The final solution mixture with a protein concentration of 20 μM at a given adjusted pH was incubated for 20 min at room temperature before optical measurements. Each spectrum was the average of four scans. The results were expressed as mean residue ellipticity ($[\theta]_\lambda$) in deg cm^2 $dmol^{-1}$. The temperatures were thermostatically controlled using a NESLAB thermostat model RTE-110 connected to a digital programming controller, and a thermocouple placed inside the optical cell. Two approaches were applied for the evaluation of effective

thermodynamic functions and the determination of cross-overlapped CD data:

(a) for temperature denaturation studies, the CD spectrum of each protein sample in the "cocktail" buffer of different pH values (from 2.5 to 12.0) was measured after 10 min of incubation at temperatures from 25 °C to 85 °C. The $[\theta]_{\lambda}$ values were recorded in steps/intervals of 5.0 ± 0.2 °C.
(b) The CD spectra of each standardized CaH solution were recorded at different temperatures from 25 °C to 85 °C (in 5 °C steps) in a wide interval of pH (2.5–12), with ~0.5 pH increments after incubation of 10 min. More precisely, the extreme values at 222 nm were digitalized and recalculated in $[\theta]_{222}$ (deg cm^2 dmol^{-1}) units.

Denaturation of CaH in water solutions in the presence of different denaturants (Gdn.HCl, urea, urea + LiCl and LiCl) was followed by CD spectroscopy. We have chosen $[\theta]_{222}$ to follow the unfolding process. CD measurements of native Hcs in 50 mM Tris-HCl buffer (pH 7.5) containing 5 mM $CaCl_2$ and 5 mM $MgCl_2$ in the presence of different concentrations of denaturants (0–8.0 M) at 25.0 °C were measured in the wavelength range 195–250 nm. The concentrations of the denaturants were stepwise increased from 0 to 8.0 M.

JASCO's multivariate Secondary Structure Estimation (SSE) program was used to analyze the CD data with more quantitative structure estimations. Using the SSE program based on the partial least squares (PLS)/principal component regression (PCA) method, the helix, β-sheet and random coil content of protein CaH have been estimated from the CD spectra. A PLS method with the latest multivariate analysis method and the PCR method are included. To minimize the residual error of the concentration, the abundance ratio of the secondary structure is calculated.

2.4 Calculation of the apparent free energy of stabilization and denaturant binding

The interaction of denaturants like urea or Gdn.HCI with proteins shows a dependence of the free energy of unfolding on the molar concentration of the denaturants that appears to be linear, at least at moderate to high denaturant concentrations where the transition typically occurs. This has led to the widespread use of the linear extrapolation method (LEM) to estimate the conformational stability of the protein in the absence of a denaturant. The application of this method gives two parameters: the free energy of unfolding at zero denaturant concentration (the intercept, $\Delta G_D^{H_2O}$) and the dependence of free energy on denaturant concentration (the slope, which has been given the symbol m) [28].

$$\Delta G_D = \Delta G_D^{H_2O} - m \times [\text{denaturant}]$$

The protein unfolds with increasing denaturant concentration because more binding sites are exposed in the unfolded form than in the folded form. Solvent denaturation curves are generally analyzed using the LEM [28], which assumes a simple linear dependence of stability on the denaturant concentration. The value for the apparent free energy of stabilization in the absence of a denaturant, $\Delta G_D^{H_2O}$, was obtained by linear extrapolation of ΔG_D, plotting to zero molar denaturant. The resulting slope of the plot of stability versus the denaturant concentration is termed the m value. The m value correlates very strongly with the amount of protein surface exposed to the solvent upon unfolding.

The molar concentration of the denaturant at which the protein is half-denatured is represented by $C_{(m)}$* (as $C_{(m)}^* = \Delta G_D^{H_2O}/m$) [28]. The $C_{(m)}$* value (or midpoint concentration) is an indicator of protein stability: large values are assumed to reflect high protein stability.

The free energy of urea/guanidine denaturation, ΔG_D, was estimated from the equation

$$\Delta G_D = -RT\ln K,$$

where K is the equilibrium constant of the denaturation process. K is calculated for each denaturant concentration according to the equation

$$K = ([\theta]_{obs} - [\theta]_N)/([\theta]_D - [\theta]_{obs}),$$

where $[\theta]_{obs}$ is the observed ellipticity at 222 nm at different concentrations of the denaturants and $[\theta]_N$ and $[\theta]_D$ are the ellipticities at the same wavelength for the folded (N) and unfolded (D) conformations of the proteins, respectively.

3 Results and discussion

The cytotoxic effect of CaH (previously HaH) is not limited to bladder cancer cell lines, but extended to human prostate cancer, ovarian carcinoma, malignant glioma, Burkitt's lymphoma and acute monocytic leukemia as well [4]. Therefore, the information on the molecular structure and conformation stability of CaH is essential.

3.1 Electron microscopic measurements of native CaH

The morphology and quaternary structure of Hcs have been identified by negative staining of the molecules by means of a transmission electron microscope [29]. The structures of the cylinder walls, collars, arcs, bridges and interfunctional unit links were gathered at 9 Å resolution to shed light on the macromolecular quaternary complex. The TEM image confirmed the quaternary structure of native Hcs, composed mainly of didecamers (20 subunits), as well as the unusual tridecamer structures found in fresh/brackish water cerithioid snails, termed mega-Hcs [1, 2, 5, 12, 13, 19, 24]. We have studied the stability and reassociation behavior of native molecules of CaH in the presence of different concentrations of Ca^{2+} and Mg^{2+} ions and pH values.

An electron micrograph of the purified negatively stained native CaH is shown in Figure 1. It is evident that the isolated material is homogeneous. No dissociated material or tubular structures were observed. Mostly, didecamers (20 subunits assembled) and a few decamers are observed (Figure 1A, native CaH), which are typical for many gastropod Hcs [2, 17, 19, 20]. Under non-physiological conditions, Hcs can lose their quaternary structure. The best way to obtain dissociation into subunits without losing the ability to reversibly bind dioxygen is to increase the pH to ~9 and remove alkaline earth cations [3]. After an overnight dialysis against 50 mM Tris-HCl buffer (pH 9.0) and 0.13 M glycine (Gly) buffer (pH 9.6), the electron microscopy analyses of dissociated CaH show a disorganized globular structure as the decameric forms dissociate into subunits (Figure 1B and C). The data show that the Gly buffer (pH 9.6) induces a strong dissociating

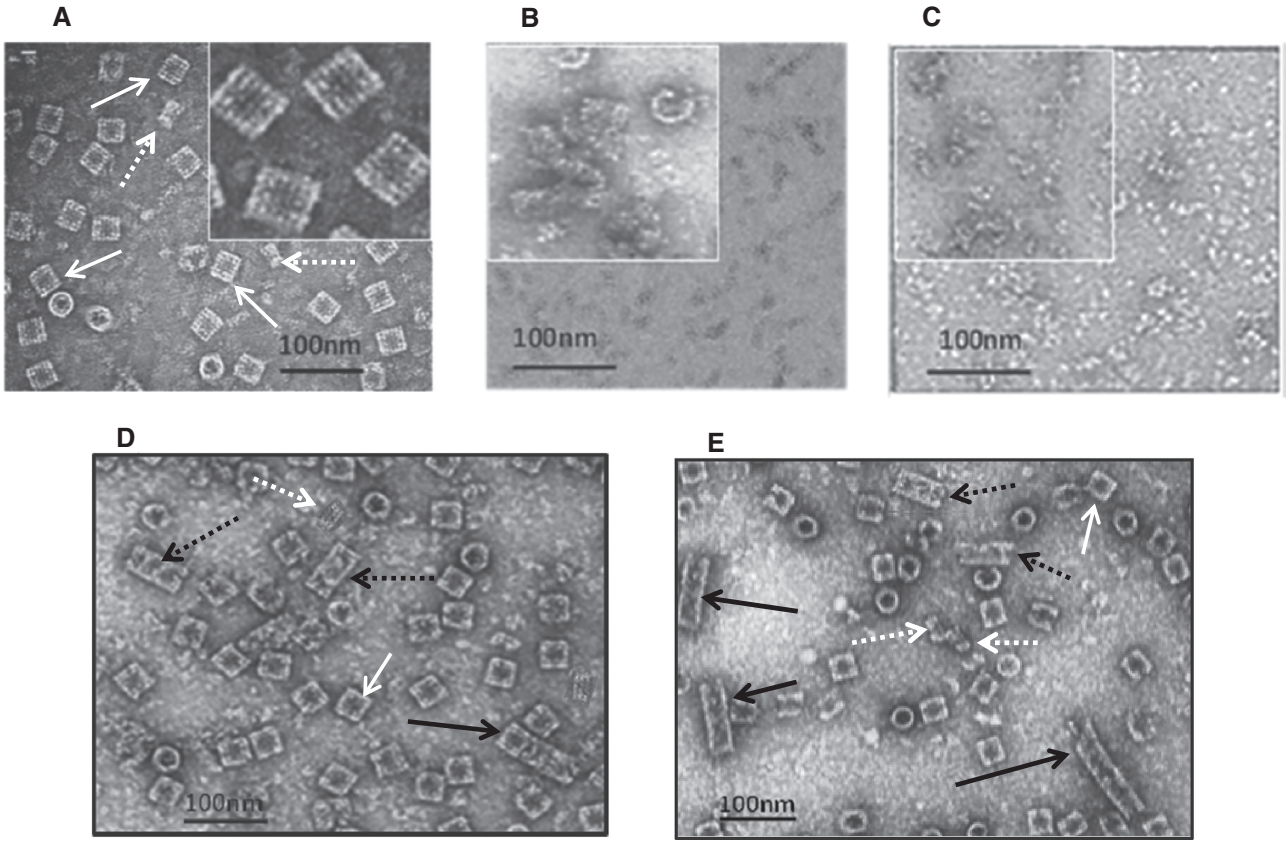

Figure 1: Gallery of electron micrographs of native CaH. (A) Electron microscopy of negatively stained native CaH in 50 mM Tris-HCl buffer (pH 7.0) containing 20 mM $CaCl_2$ and 10 mM $MgCl_2$. The images show top (circles) and lateral (rectangles) views of the molecule. Primarily, didecamers (white arrows) and few decamers (white dash arrows) are observed. The insert figure shows the characteristic didecameric forms of CaH, with subunits arranged in layers. (B) Dissociated protein in 50 mM Tris-HCl buffer (pH 9.0). (C) Dissociated protein in 0.13 M Gly/NaOH buffer at pH 9.6. (D) Reassociated CaH after 3 days of dialysis against SB (pH 7.0) containing 50 mM Tris-HCl buffer, 50 mM $CaCl_2$ and 50 mM $MgCl_2$. (E) Reassociated CaH after 3 days of dialysis against SB containing 50 mM Tris-HCl buffer (pH 7.0) containing 100 mM $CaCl_2$ and 100 mM $MgCl_2$. Mainly, didecamers (white arrows), tridecamers (black dash arrows) and multidecamers of varying lengths (black arrows) are observed in (D) and (E). Scale bar: 100 nm.

environment and CaH mainly occurs as "loose" and/or "compact" monomeric subunits. On the alkaline side of the pH/stability region, native CaH successively dissociates into 10 and 20 subunits. The subunits do not dissociate further under these mild conditions, similar to *H. lucorum* and *H. pomatia* Hcs, *R. venosa* hemocyanin (RvH) and keyhole limpet hemocyanin (KLH) [16, 17, 19, 20, 24]. The electron microscopic analysis of negatively stained dissociated CaH (Figure 1B and C) shows a disorganized globular structure. After changing the conditions with the stabilizing buffer (SB) (pH 7.0) containing 50 mM $CaCl_2$ (Figure 1D), the obtained structural subunits mostly reassociate to didecamers (white arrows) and a few decamers (dash white arrows) and tridecamers (black dash arrows). The typical Hc tridecamer observed in the CaH (Figure 1D) and previously in the subunit KLH2 and native HlH is a transient state between the comparatively stable didecamers and larger multidecamers [13, 17, 24]. By increasing the concentrations of both divalent ions, Ca^{2+} and Mg^{2+}, to 100 mM, the reassociation is increased, and not only didecamers (white arrows) but also multidecamers of varying lengths (black arrows) are produced. The multidecamers consist of a "nucleating" didecamer with attached decamers at one or two sides (Figure 1E). The observed reassociation of CaH after a 3-day dialysis in 50 mM Tris buffer, containing 100 mM $CaCl_2$ and 100 mM $MgCl_2$ (pH 7.0), does not lead to the formation of long tubular polymers as previously published for both subunits RvH1 [19, 20] and KLH2 [24] in the same conditions. The higher concentrations of the Ca^{2+} and Mg^{2+} ions (100 mM each) were more efficient and led to a more rapid reassociation of native CaH, yielding long stable multidecamers. A similar reassociation behavior was observed in the native HlH and the subunits KLH2 and RvH2 [17–19, 24]. We have not observed mega-Hc tridecamers as was discovered in fresh/brackish water cerithioid snails (*Leptoxis*, *Melanoides* and *Terebralia*). The cerithioid tridecamer comprises two typical decamers based on the canonical 400-kDa subunit, flanking a central "mega-decamer" composed of 10 unique ~550-kDa subunits [13, 14].

3.2 CD studies

Protein secondary structural information of the native CaH was derived from CD signals in the "far-UV" spectral region between ~250 and 190 nm due to the amide chromophores of the peptide bonds. The CD spectrum of the native CaH shows two distinct negative Cotton effects at 208 and 222 nm due to the α-helix and β-sheet structures of the protein, similar to KLH and *H. lucorum* hemocyanin [17, 24–26]. However, the changes of $[\theta]_{222}$ (especially small ones) are related not only to changes in polypeptide helicity but more generally to changes in interactions and orientations of protein peptides [20].

3.2.1 Thermal stability of CaH in buffers with different pH values

The conformational changes of native CaH were measured in buffers with different pH values via their CD spectra (Figure 2). A characteristic feature is the *T*-induced changes within a wide temperature interval of 25 °C–85 °C (Figure 3A). A drastic decrease in negative ellipticity was observed at temperatures above 50 °C. Another feature is the irreversibility of common "end states" with a relatively similar disordered structure. The amplitude $\Delta[\theta]_N - \Delta[\theta]_D$ for curves at a different pH is decreased upon moving to extreme pH values (Figure 3A). The relatively small changes of initial $[\theta]_{222}$ at high temperatures indicate that the main part of the structural elements is preserved, especially at neutral pH and even at high temperatures (Figure 3A and B). The data for the secondary structure of CaH estimated from the CD spectra, using the SSE program and the PLS multivariate analysis at $T = 25$ °C and $T = 100$ °C (at pH 7.0), indicated a decrease in α-helix from 24.9% to 12.5%, in β-turn from 29.5% to 15.8%, in random coil conformation from 34.5% to 28.0%, and an increase in β-sheet from 11.0% to 32.0%. So, the thermal-induced unfolding of native CaH shows quantity of the decrease in α-helix, but the increase in β-sheet. The thermal-induced unfolding of native CaH was found to be irreversible in nature. The thermal denaturation of other gastropod Hcs from *R. venosa*, *Megathura crenulata* and *Viviparus ater*

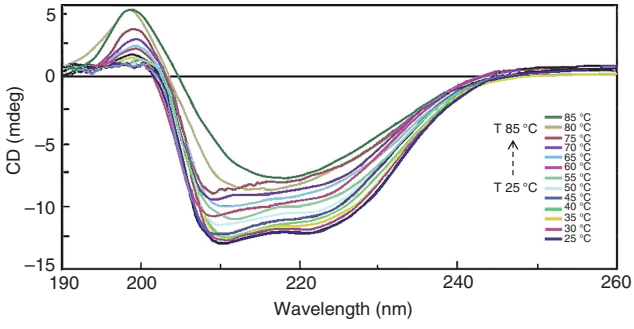

Figure 2: CD spectra of native CaH ($A_{278} = 0.360$) recorded at different values of *T* (25 °C–85 °C), at pH 7.0, in the range between 190 and 260 nm. Two negative Cotton effects at 222 and 208 nm were digitalized in the CD spectra of the Hc solutions of the native CaH.

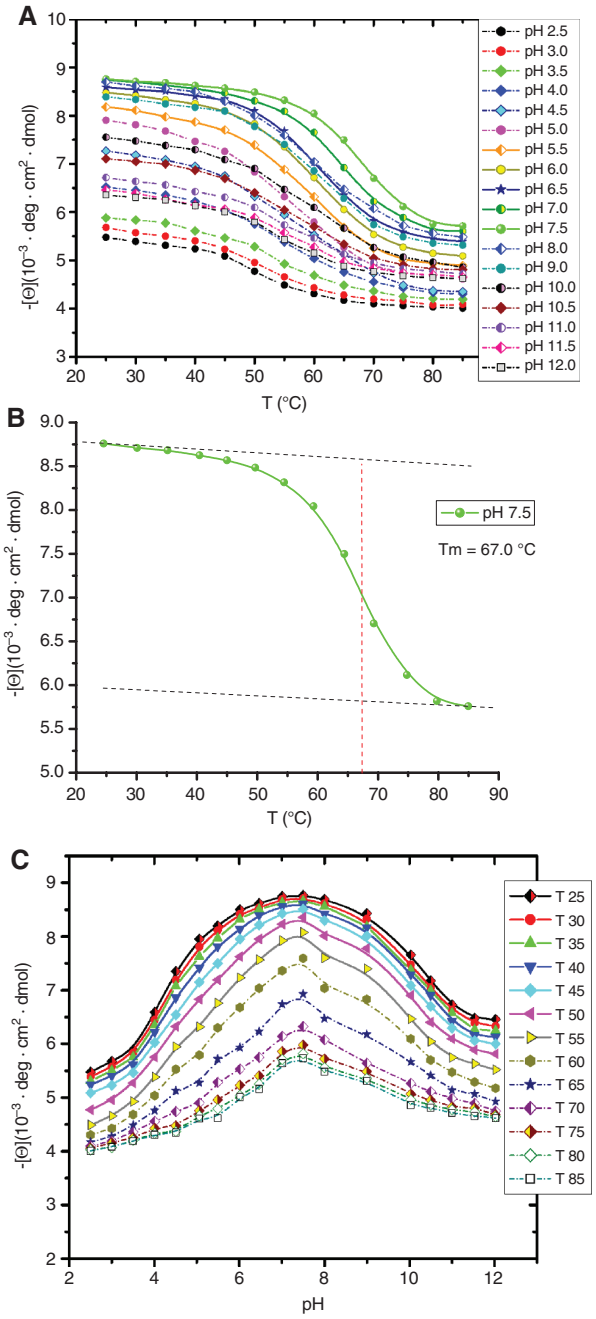

Figure 3: (A) Influence of pH on $[\theta]_{222}$ of CaH at different temperatures. Part of the curves considered to be reversible (in solid) is locked in vertical dashed lines. (B) The melting temperature at pH 7.5 (T_m = 67.0 °C) for native CaH. (C) Influence of temperature on the unfolding of native CaH at different pH measured by CD spectra at 222 mn. The *T*-induced changes are obtained over a wide temperature interval (25.0 °C–85.0 °C) at fixed pH (2.5–12).

and arthropod Hcs from *Palinurus vulgaris* and *Eurypelma californicum* was also found to be irreversible, probably due to an aggregation of the giant biomolecules [20, 22, 24–26, 30, 31].

Thermostability of the undissociated native CaH was investigated by following the changes in ellipticity at 222 nm with temperature (Figure 2). The thermal denaturation was irreversible due probably to aggregation, and the thermostability was characterized by the transition or the "melting" temperature, T_m, which is the midpoint of the sigmoidal denaturation curves (Figure 3B). Molluscan Hcs are thermostable proteins with melting temperatures in the range of 50.0 °C–85.0 °C. The melting temperature at pH 7.5 for native CaH (T_m = 67.0 °C) correlates with the thermostability of native KLH (T_m = 67.0 °C) [25], HtH (T_m = 76.0 °C) [21] and the Hc from *V. ater* (T_m = 77.0 °C) [22]. The native CaH has more thermostability compared to the native RvH (T_m = 58.1 °C, at pH 7.0) as well as the structural subunits KLH1 (T_m = 56.0 °C, at pH 8.0), KLH2 (T_m = 52.0 °C, at pH 8.0), RvH1 (T_m = 55.6 °C, at pH 7.5) and RvH2 (T_m = 55.0 °C, at pH 8.0) [20, 26]. The larger T_m values of the native Hcs compared to their subunits are an excellent indication of their stabilization caused by oligomerization introducing additional factors like non-ionic forces (intra-subunit, hydrophobic and hydrogen-bonded networks and carbohydrate moiety interactions). The Hcs of the lobsters *P. vulgaris* (T_m = 63.1 °C) [30] and *Nephrops norvegicus* (T_m = 55.0 °C) [32] are much less heat resistant compared to the native CaH, while the Hc from the tarantula *E. californicum* has extreme thermostability (T_m = 91.0 °C) [31] (see Table 2).

3.2.2 Influence of pH on dichroic spectra of CaH at 222 nm at different temperatures

For native CaH, the $[\theta]_{222}$/pH plots (Figure 3C) represent a set of smooth and partially bell-shaped curves with maxima between pH 6.0–8.5 and non-symmetric acidic and alkaline extremes, but without any obvious sigmoid feature at extreme pH. At increasing temperature above 50 °C, the character of the curves change, showing a slight peak in the pH range 6.5–8.0, indicating the presence of two ionization processes (due to the carboxylates and imidazoles), with an opposing influence on the left (L, acidic) and right (R, alkaline) limbs of $[\theta]_{222}$ (pH), similar to what was observed for RvH1 and RvH2 [20]. Both pH-acid and pH-alkaline denaturations are poorly presented in all curves at extreme pH regions (Figure 3C), which can be explained by an increased stability due to quaternary structure of the native CaH. In the alkaline part (pH 8–12), relative changes of pH transitions are too small and non-cooperative (within a wide pH interval), indicating that alkaline denaturation cannot be achieved as a reversible process. This is supported by comparison with the data

from other molluscan Hcs [20, 25, 26]. The relative changes were found to be small and almost non-cooperative (in the vicinity of pH 2.5), indicating that acidic denaturation cannot be achieved as a reversible process for this intermediate species. However, overall, for multimeric intact Hc, a small interval of partial reversibility in the acidic region close to pH 5.5 at 25 °C is possible. Thus, it can be concluded that reversibility is possible in the pH interval in an acidic range, indicating the involvement of titrable groups responsible for structural stability. Previously, a similar effect of acidic and alkaline pH transitions on dichroic spectra was monitored for RvH and KLH [20, 25, 26]. Denaturation studies of other native gastropod Hcs [20–22, 25, 26] by pH indicate that it may be difficult to distinguish between effects on the quaternary structure of the oligomeric protein (initial dissociation) and those on the tertiary and secondary structures (i.e. subunit unfolding). Obviously, the mechanism of thermal denaturation of multimeric intact CaH has a complicated character, and the process of thermal unfolding is irreversible. Thus, neither real thermodynamic data nor structurally related activation parameters could be obtained. A similar situation was also observed for the analysis of thermal unfolding of native RvH and its subunits and KHL [20, 23–26].

The high sensitivity of the CD experiments allows the use of much lower concentrations to monitor *T* (°C)- and pH-dependent unfolding of the proteins (compared with DSC) and to determine small pH and *T* (°C) intervals in which the processes take place reversibly [20]. Two independent sets of experiments, with 14–15 samples each, were collected for CaH: $[\theta]_{222}$ as a function of *T* (°C) at different pH and $[\theta]_{222}$ as a function of pH at different *T* (°C). The total reversibility of the system suggests independence of the final states from the path(s) of their realization. The experimental matrix $[\theta]_{exp(T)}$ was converted to the calculated $[\theta]_{cal(pH)}$, and the matrix $[\theta]_{exp(pH)}$ to the $[\theta]_{cal(T)}$. Reversibility of the pH-*T* denaturation is the base paradigm of protein self-organization, and the applicability of the reversible thermodynamics approach can be used for the evaluation of its stability [20]. The lines connect the *T*-pH points with equal reversibility (%) as 100 (1), 96 (2), 92 (3), 88 (4) and 84 (5). A "phase diagram," plotted as a *T*-pH grid of $[\theta]_{222}$, represents the pH-induced conformational changes of CaH (Figure 4). From the pH-*T* diagram of Figure 4, the multimeric intact CaH structure has a very small interval of partial reversibility at acidic pH range close to pH 5.5–6.5 at temperatures below 60 °C, as well as perturbance in the region of pH 7.0. Probably, the Hc chains agglomerate at weak acidic pH, which is typical for gastropod hemolymph when most carboxylates are protonated, and thus, the repulsive interactions are diminished. Apparently, thermal denaturation of the native

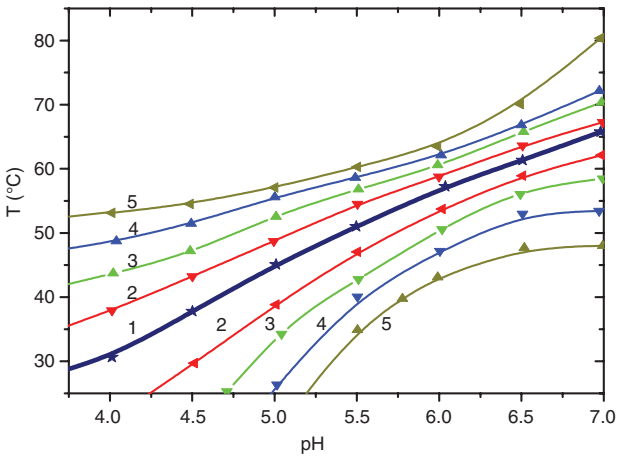

Figure 4: The curves were obtained by $[\theta]_{222}(T)$–$[\theta]_{222}$(pH) functions, showing the reversibility zones for the native CaH. Lines connect the pH-*T* points with the same % reversal as 100% (1), 96% (2), 92% (3), 88% (4) and 84% (5).

molecule CaH is an irreversible process, and their real thermodynamic data cannot be obtained. The thermal- and pH-induced denaturation of native CaH could be accompanied by dissociation into subunits because CaH is an oligomeric protein [4, 15]. The stability of native Hcs, shown by coupled *T* and pH transitions (acid and alkaline denaturation), was explained by the formation of quaternary structures, which introduces additional factors, namely, non-ionic forces, as an intra-subunit, hydrophobic and hydrogen-bonded networks of carbohydrate moiety interactions [20].

3.2.3 Conformational stability of native CaH in the presence of different chemical denaturants

Stability studies of proteins are of increasing importance for biotechnological processes or medical biologics. Incorrect folding by an unfavorable environment will change the protein structure and destroy the intended functional purpose. Denatured states of proteins play an important role in protein folding, transport across membranes and proteolysis [33], which is the reason for the increasing interest in these states during the past few years. The unfolding reaction of native CaH in the presence of increasing concentrations of Gdn.HCl, urea, urea + LiCl and LiCl was followed by CD spectroscopy. We have chosen $[\theta]_{222}$ to follow the unfolding process. The protein concentration in the cuvette was around 0.26 mg/mL in 0.05 M Tris buffer (pH 7.5) at 25 °C. The obtained results were analyzed assuming a two-state mechanism, and the unfolded protein was plotted as a function of denaturant concentration. From the data in the transition region and using the linear extrapolation model,

the thermodynamic parameters were determined (Figure 5, Table 1). The free energy of stabilization in water, $\Delta G_D^{H_2O}$, even apparent as here, is a quantitative measure for the protein stability in water solutions, the free energy change for the reaction "globular conformation ↔ random coil conformation" in the absence of a denaturant. The mechanism of denaturation involves modification of the water structure by a denaturant and its interaction with the peptide groups [34, 35]. Gdn.HCl and urea are the commonly used denaturants to determine the free energy of protein stabilization in water [33].

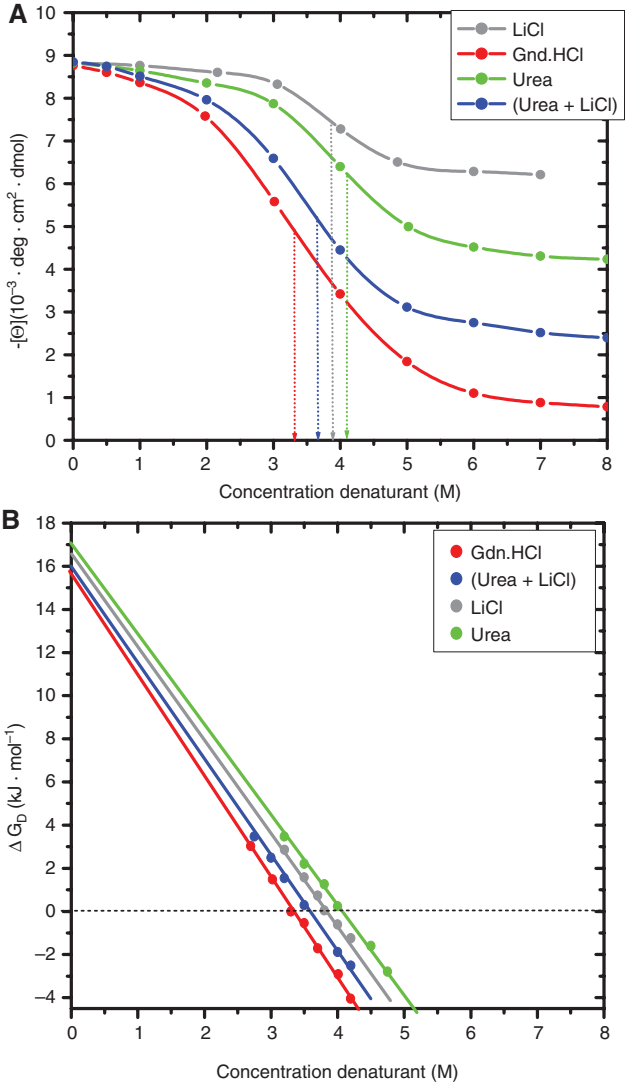

Figure 5: (A) Unfolding of the CaH (0.26 mg/mL) at pH 7.5 and $T = 25$ °C by different chemical denaturants: LiCl, urea, urea + LiCl and Gdn.HCl, determining the ellipticity at 222 nm. (B) The panel shows the dependence of free energy for unfolding of the native CaH as a function of each of the four denaturants. The data in the transition region can be extrapolated to determine $\Delta G_U(H_2O)$ using the LEM.

Table 1: Unfolding of the CaH at pH 7.5 and 25.0 °C by increasing concentrations of denaturants: Gdn.HCl (M), (urea + LiCl) (M each), urea (M) and LiCl (M), using CD.

	Denaturant	ΔG_D^{H2O} (kJ·mol^{-1})	$C_{(m)}$* (M)	m (kJ·mol^{-1}·M)
1	Gdn.HCl	15.48	3.32	4.663
2	Urea + LiCl	15.82	3.62	4.370
3	LiCl	16.48	3.90	4.226
4	Urea	16.95	4.11	4.124

The concentration of the denaturants is in the range 0.0–8.0 M.

The influence of increasing concentrations of Gdn.HCl on the negative ellipticity at 222 nm is shown in Figure 5A. The ellipticity is retained in the range of 0–2 M Gdn.HCl concentration. An extensive decrease in ellipticity was observed from 2.0 to 5.0 M Gdn.HCl. Similar curves were obtained for the aggregated *Rapana* Hc and its structural subunits and KLH, as the ellipticity is retained in the range of 0–1.5 M Gdn.HCl concentration [18, 24]. The data from the SSE program based on the PLS/PCA method confirm the changes in the secondary structure of the protein observed with an increase in the concentration from 0–8 M Gdn.HCl: more specifically, a decreased ratio for α-helix from 24.9% to 0.2%, for β-turn from 29.5% to 0% and random coil conformation from 34.5% to 18.4%, but an increase in β-sheet from 11% to 82%. From the data, it is apparent that Gdn.HCl is an excellent denaturant, breaking all types of non-covalent interactions in the protein. Gdn.HCl is a salt and therefore expected to ionize in an aqueous solution. At low concentrations, Gdn^+ and Cl^- ions are presumed to mask the positively and negatively charged amino acid side chains, thereby reducing or even totally eliminating any stabilizing or destabilizing electrostatic interactions. The binding of the Gdn^+ ions to the proteins is presumed to predominate and to push the equilibrium toward the unfolded state [36]. A slight increase in protein stability in the presence of low Gdn.HCl concentration has been observed for different proteins. At high concentrations, Gdn.HCl becomes a denaturant, regardless of the types of electrostatic interactions present in the protein [37, 38]. Thus, the random coil analogs that differed only in terms of their electrostatic interactions had the same apparent stability. These results suggest that the estimates of protein stability (dG_u) by Gdn.HCl denaturation studies would likely be a relative measure for the contributions of hydrophobic interactions. From the transition curve (Figure 5A), the midpoints of transition show that Gdn.HCl brings about protein denaturation at a lesser concentration as compared to LiCl and urea.

Table 2: Values of melting temperature (T_m) and free energy of stabilization in water ($\Delta G_D^{H_2O}$) at pH 7.5 and 25 °C for various Hcs.

Hc species	T_m (°C)	$\Delta G_D^{H_2O}$ Gdn.HCl
Molluscs		
Native CaH (*Cornu aspersum* Hc)	67.0	15.5 kJ mol^{-1}
Native KLH (*Megathura crenulata*)	67.0 [26]	25.9 kJ mol^{-1} [24]
KLH1 subunit	56.0 [26]	17.6 kJ mol^{-1} [24]
KLH2 subunit	52.0 [26]	22.6 kJ mol^{-1} [24]
Native HtH (*Haliotis tuberculata*)	76.0 [23]	No data
Viviparus ater Hc	77.0 [22]	12.6 kJ mol^{-1} [21]
Native *Rapana thomasiana* Hc	79.0 [23]	21.6 kJ mol^{-1} [21]
Native *Rapana venosa* Hc	58.1 [20]	22.6 kJ mol^{-1} [18]
RvH1 subunit	55.6 [20]	16.3 kJ mol^{-1} [18]
RvH2 subunit	55.0 [20]	18.4 kJ mol^{-1} [18]
Helix aspersa maxima (isoform β–HaH)	79.88 [27]	No data
Arthropods		
Maia squinado Hc	76.0 [23]	12.6 kJ mol^{-1} [21]
Carcinus maenas Hc	72.0 [23]	11.4 kJ mol^{-1} [21]
Palinurus vulgaris Hc	63.1 [30]	12.2 kJ mol^{-1} [21]
Eurypelma californicum Hc	91.0 [31]	No data
Nephrops norvegicus Hc	55.0 [32]	No data
Homarus americanus Hc	81.0 [21]	13.5 kJ mol^{-1} [21]

The ionic nature of Gdn.HCl masks the electrostatic interactions in proteins, a phenomenon that was absent in the case of urea. Thus, Gdn.HCl and urea denaturations may give vastly different estimates of protein stability, depending on how important electrostatic interactions are to the protein [39]. The "direct electrostatic mechanism" suggests that urea interacts directly with the protein backbone via hydrogen bonds and other electrostatic interactions with charged and polar side chains predominantly [40]. Our results from the CD experiments with urea also show that the secondary structure of the protein is affected with an increase in the concentration to 8.0 M, but in a different way. After incubation for 24 h in different concentrations of urea (0–8.0 M, breaking internal hydrogen bonds and solubilizing hydrophobic groups), the decrease in negative ellipticity at 222 nm indicates a significant unfolding of the structure of CaH, but not denaturation of the whole molecule CaH (Figure 5B). The data from multivariate SSE program and PLS analysis show a decrease in α-helix from 24.9% to 16.8%, in β-turn from 29.5% to 20.6% and in random coil conformation from 34.5% to 29.9% with increasing urea concentration range (0–8.0 M); an increase in β-sheet from 11% to 32.6% is observed. The protein stability by urea denaturation studies is a relative measure of the contributions of electrostatic interactions to the stability of CaH.

Increasing the effectiveness of urea as a denaturant to correspond to Gdn.HCl could be achieved by increasing the ionic strength of the solution by introducing LiCl (see Figure 5A). This suggests that Gdn.HCl affects hydrophobic and ionic interactions simultaneously, while urea affects almost solely hydrophobic interactions [36]. The sigmoid curve of titration with LiCl suggests Li^+ binding to CaH. Remarkable is the special shape of the CaH titration curve with LiCl, not to be caused by a pure electrolyte, but by Li^+ binding to the protein forming "lithium bonds" [41, 42]. Using LiCl and urea simultaneously as a denaturation agent, we were able to mimic the bifunctional ability of Gdn.HCl [36], providing a new tool to assist the correct refolding of unfolded proteins.

In our studies, we demonstrate that native CaH unfolding with urea + LiCl is similar to unfolding in the presence of Gdn.HCl (Figure 5B, Table 1). The quantitative comparison of Gdn.HCl by urea + LiCl unfolding could serve as a new tool to explore refolding pathways by varying the concentrations of urea or LiCl, independently. As further detailed studies are needed, it is at present time very difficult to elucidate the different effects of two denaturants on the hydrogen bonding of the protein structure. The unfolded protein was plotted as a function of four denaturants in increasing concentrations. The thermodynamic parameters were determined (Table 1). The conformational stability of native CaH as a function of concentration of used denaturants was determined by the free energy of protein stabilization in water ($\Delta G_D^{H_2O}$). The values of $\Delta G_D^{H_2O}$ for native CaH are within ranges from 15.48 to 16.95 kJ mol^{-1} (or 3.70–4.05 kcal mol^{-1}) (Figure 5B, Table 1). These results are in good agreement with the values of other investigated Hcs (Table 2). Apparently, the midpoints of protein unfolding in the presence of different denaturants are in the region of 3.2–4.11 M. (Figure 5B). The data in Figure 5B and Table 1 illustrate that the four denaturants result in much the same value for $\Delta G_D^{H_2O}$ (with only 1.47 kJ mol^{-1} or 0.35 kcal mol^{-1} separating the values). In actuality, this good agreement in solutions of Gdn.HCl and urea compounds that differ greatly in ionic character, solution properties and efficacy in denaturation gives compelling evidence that $\Delta G_D^{H_2O}$ is a property of the protein system, essentially independent of the denaturant. A similar result, showing good agreement between $\Delta G_D^{H_2O}$ values obtained from the linear extrapolation using three denaturants with phenylmethanesulfonyl α-chymotrypsin, was observed from Santoro and Bolen [43].

Understanding the conformational changes that result from various treatments has shed some light on the structural alterations and loss of function which can result due to exposure of denaturants and, thus, affect the normal functioning of the protein.

4 Conclusion

The study of Hc conformational stability is of fundamental interest to our understanding of the structure-function relationships in these dioxygen carriers. Based on coupled *T* and pH transitions, the stability of native oligomeric Hc from *C. aspersum* is explained by the formation of quaternary structures, introducing additional factors, like non-ionic forces. Apparently, thermal denaturation of the native CaH is an irreversible processes, and its real thermodynamic data cannot be obtained under the given conditions. This type of behavior was shown by other authors for the other Hcs [17, 21–26].

For the first time, the unfolding of native CaH in water solutions in the presence of four different denaturants is described in the literature. The conformational stability of the native didecameric aggregates of CaH toward various denaturants (pH and Gdn.HCl) indicates that hydrophilic and polar forces stabilize the quaternary structure, similar to KLH and RvH. However, it may be difficult to distinguish between the effects on the quaternary structure of the oligomeric protein (initial dissociation) and those on the tertiary and secondary structure (i.e. subunit unfolding).

The presented results will facilitate the further investigation of the properties and potential biomedical applications of CaH.

Acknowledgments: This work was supported by the research grant Project BG05M2OP001-1.002-0019: "Clean technologies for sustainable environment – water, waste, energy for circular economy" (Clean & Circle), for development of a Centre of Competence and by the Bulgarian Ministry of Education and Science under the National Research Program "BioActivMed" approved by DCM № 658/14.09.2018.

References

1. Decker H, Hellmann N, Jaenicke E, Lieb B, Meissner U, Markl J. Minireview: recent progress in hemocyanin research. Integr Comp Biol 2007;47:631–44.
2. Markl J. Evolution of molluscan hemocyanin structures. Biochim Biophys Acta 2013;1834:1840–52.
3. Van Holde KE, Miller KI. Hemocyanins. Adv Protein Chem 1995;47:1–81.
4. Antonova O, Dolashka P, Toncheva D, Rammensee H-G, Floetenmeyer M, Stevanovic S. In vitro antiproliferative effect of *Helix aspersa* hemocyanin on multiple malignant cell lines. Z Naturforsch C 2014;69:325–34.
5. Coates CJ, Nairn J. Diverse immune functions of hemocyanins. Dev Comp Immunol 2014;45:43–55.
6. Arancibia S, Salazar F, Becker MI. Hemocyanins in the immunotherapy of superficial bladder cancer. In: Canda A, editor. Bladder cancer – from basic science to robotic surgery. Croatia: In Tech Open, Chapter 11, 2012:221–42.
7. Dolashka P, Velkova L, Iliev I, Beck A, Dolashki A, Yossifova L, et al. Antitumor activity of glycosylated molluscan hemocyanins via Guerin ascites tumor. Immunol Invest 2011;40:130–49.
8. Dolashka P, Velkova L, Shishkov S, Kostova K, Dolashki A, Dimitrov I, et al. Glycan structures and antiviral effect of the structural subunit RvH2 of *Rapana* hemocyanin. Carbohydr Res 2010;345:2361–7.
9. Dolashka P, Dolashki A, Van Beeumen J, Floetenmeyer M, Velkova L, Stevanovic S, et al. Antimicrobial activity of molluscan hemocyanins from *Helix* and *Rapana* snails. Curr Pharm Biotechnol 2016;17:263–70.
10. Lamm DL. Laboratory and clinical experience with keyhole limpet hemocyanin (Immunocothel) in superficial bladder cancer. J Urol 2003;10:18–21.
11. Zanjani NT, Saksena MM, Dehghani F, Cunningham AL. From ocean to bedside: the therapeutic potential of molluscan hemocyanins. Curr Med Chem 2018;25:2292–303.
12. Zhuang J, Coates CJ, Zhu H, Zhu P, Wu Z, Xie L. Identification of candidate antimicrobial peptides derived from abalone hemocyanin. Dev Comp Immunol 2015;49:96–102.
13. Lieb B, Gebauer W, Gatsogiannis C, Depoix F, Hellmann N, Harasewych MG, et al. Molluscan mega-hemocyanin: an ancient oxygen carrier tuned by a ~550 kDa polypeptide. Front Zool 2010;7:14.
14. Gatsogiannis C, Hofnagel O, Markl J, Raunser S. Structure of mega-hemocyanin reveals protein origami in snails. Structure 2015;23:93–103.
15. Gielens C, De Sadeleer J, Preaux G, Lontie R. Identification, separation and characterization of the hemocyanin components of *Helix aspersa*. Comp Biochem Physiol 1987;88B:181–6.
16. Lontie R. Components, functional units, and active sites of *Helix pomatia* hemocyanin. Life Chem Rep Suppl 1983;1:109–20.
17. Velkova L, Dimitrov I, Schwarz H, Stevanovic S, Voelter W, Salvato B, et al. Structure of hemocyanin from garden snail *Helix lucorum*. Comp Biochem Physiol B Biochem Mol Biol 2010;157:16–25.
18. Dolashka P, Genov N, Parvanova K, Voelter W, Geiger M, Stoeva S. *Rapana thomasiana* grosse (gastropoda) haemocyanin: spectroscopic studies of the structure in solution and the conformational stability of the native protein and its structural subunits. Biochem J 1996;315:139–44.
19. Dolashka-Angelova P, Schwarz H, Dolashki A, Stevanovic S, Fecker M, Saeed M, et al. Oligomeric stability of *Rapana venosa* hemocyanin (RvH) and its structural subunits. Biochim Biophys Acta 2003;1646:77–85.
20. Dolashki A, Velkova L, Atanasov B, Voelter W, Stevanovic S, Schwarz H. Reversibility and "pH–T phase diagrams" of *Rapana venosa* hemocyanin and its structural subunits. Biochim Biophys Acta 2008;1784:1617–24.
21. Hristova R, Dolashka P, Stoeva S, Voelter W, Salvato B, Genov N. Spectroscopic properties and stability of hemocyanins. Spectroch Acta Part A 1997;53:471–8.
22. Georgieva D, Stoeva S, Voelter W, Genov N. *Viviparus ater* hemocyanin: investigation of the dioxygen-binding site and stability of the oxy- and apo-forms. Z Naturforsch C 2001;56c:843–7.

23. Georgieva DN, Stoeva S, Ali SA, Abbasi A, Genov N, Voelter W. Circular dichroism study of the hemocyanin thermostability. Spectrochim Acta A 1998;54:765–71.
24. Schütz J, Dolashka-Angelova P, Abrashev R, Nikolov P, Voelter W. Isolation and spectroscopic characterization of the structural subunits of keyhole limpet hemocyanin. Biochim Biophys Acta 2001;1546:325–36.
25. Varshney A, Ahmad B, Rabbani G, Kumar V, Yadav S, Khan RH. Acid-induced unfolding of didecameric keyhole limpet hemocyanin: detection and characterizations of decameric and tetrameric intermediate states. Amino Acids 2010;39:899–910.
26. Dolashki A, Schutz J, Hristova R, Voelter W, Dolashka P. Spectroscopic properties of non-glycosilated functional unit KLH2-c of keyhole limpet hemocyanin. World J Agric Sci 2005;1:129–36.
27. Todinova S, Raynova Y, Idakieva K. Calorimetric study of *Helix aspersa* maxima hemocyanin isoforms. J Anal Methods Chem 2018;2018:8450792.
28. Pace CN, Shaw KL. Linear extrapolation method of analyzing solvent denaturation curves. Proteins 2000;4:1–7.
29. Meissner U, Gatsogiannis C, Moeller A, Depoix F, Harris R, Markl J. Comparative 11 Å structure of two molluscan hemocyanins from 3D cryo-electron microscopy. Micron 2007;38:754–65.
30. Guzmán-Casado M, Parody-Morreale A, Mateo PL, Sánchez-Ruiz JM. Differential scanning calorimetry of lobster haemocyanin. Eur J Biochem 1990;188:181–5.
31. Sterner R, Vogl T, Hinz HJ, Penz F, Hoff R, Föll R, et al. Extreme thermostability of tarantula hemocyanin. FEBS Lett 1995;364:9–12.
32. Coates C, Nairn J. Hemocyanin-derived phenoloxidase activity: a contributing factor to hyperpigmentation in *Nephrops norvegicus*. Food Chem 2013;140:361–9.
33. Dill KA, Shortle D. Denatured states of proteins. Annu Rev Biochem 1991;60:795–825.
34. Nandi PK, Robinson DR. Effects of urea and guanidine hydrochloride on peptide and nonpolar groups. Biochemistry 1984;23:6661–8.
35. Prakash V, Loucheux C, Scheufele S, Gorbunoff M, Timasheff S. Interactions of proteins with solvent components in 8 M urea. Arch Biochem Biophys 1981;210:455–64.
36. Monera OD, Kay CM, Hodges RS. Protein denaturation with guanidine hydrochloride or urea provides a different estimate of stability depending on the contributions of electrostatic interactions. Protein Sci 1994;3:1984–91.
37. Matsubara M, Nohara D, Sakai T. Difference between guanidinium chloride and urea as denaturants of globular proteins: the possibility of application to improved refolding processes. Chem Pharm Bull 1992;40:550–2.
38. Monera OD, Zhou NE, Kay CM, Hodges RS. Comparison of antiparallel and parallel two-stranded alpha-helical coiled-coils. Design, synthesis, and characterization. J Biol Chem 1993;268:19218–27.
39. Roseman M, Jencks WP. Interactions of urea and other polar compounds in water. J Am Chem Soc 1975;97:631–40.
40. Rossky PJ. Protein denaturation by urea: slash and bond. Proc Natl Acad Sci USA 2008;105:16825–26.
41. Berski S, Latajka Z. Comparison of lithium and hydrogen bonds in (X···Li···X)- and (X···H···X)- (XF, Cl and Br) complexes: topological analysis of electron localization function. Int J Quant Chem 2002;90:1108–20.
42. Scheiner S. Hydrogen bonding: a theoretical perspective. New York: Oxford University Press, 1997.
43. Santoro MM, Bolen DW. Unfolding free energy changes determined by the linear extrapolation method. 1. Unfolding of phenylmethanesulfonyl α-chymotrypsin using different denaturants. Biochemistry 1988;27:8063–8.